Agricultural and Forest Meteorology 171–172 (2013) 234–248

Contents lists available at SciVerse ScienceDirect

Agricultural and Forest Meteorology

journal homepage: www.elsevier.com/locate/agrformet

Climate change impacts on regional winter wheat production in main wheat production regions of China

Zunfu Lv, Xiaojun Liu, Weixing Cao, Yan Zhu*

National Engineering and Technology Center for Information Agriculture, Jiangsu Key Laboratory for Information Agriculture, Nanjing Agricultural University, 1 Weigang Road, Nanjing, Jiangsu 210095, PR China

ARTICLE INFO

Article history:
Received 14 October 2012
Received in revised form
14 December 2012
Accepted 17 December 2012

Keywords:
GCM
WheatGrow model
Climate change impacts
Wheat yield
IWUE
ET

ABSTRACT

Wheat is the second primary crop in China. Wheat production in China is an important component for national food security. The combination of high-resolution Global Climate Model (GCM) and WheatGrow model was used to assess the effects of climate change on wheat yields in the main wheat production regions of China. With the application of many techniques including the downscaling of meteorological data, rasterizing of sowing date, parameterization of region cultivar and vectorization of soil data, the spatial data in study area is divided into homogeneous grids with the resolution of $0.1^\circ \times 0.1^\circ$. The grid is taken as the basic simulation unit, and each grid has a complete set of input data (meteorological, soil, management and varieties). Regional productivities are simulated with WheatGrow for each grid cell under scenarios of climate-change. There is an advance in flowering date in future climate compare to 2000s, but with a more homogeneous pattern for the whole producing region. The changes in grain filling period are relatively stable. Under rain-fed conditions, wheat yield is reduced in the north regions of China in three future periods, while wheat yield increases in the south regions of China. Under full-irrigation conditions, irrigated wheat yields will increase in almost all regions of whole producing region. The spatial pattern of evapotranspiration change is quite similar to that of yield change under rain-fed and full-irrigation conditions. The correlation between wheat yield and evapotranspiration (ET) increases to 0.96 and 0.51 ($p < 0.01$) under rain-fed and full-irrigation conditions, respectively. The irrigation water use efficiency (IWUE) will decrease under three time slices in 2030s, 2050s and 2070s in western Shandong, southern Sichuan, as well as northern Henan, Shanxi and Shaanxi, while IWUE will increase under scenarios of climate-change in other areas. The results revealed that the increase in effective irrigation in the future would help to increase the ET and further improve the wheat yield in the northern regions of China, and the limited water should be mad full use of in the regions with relatively high IWUE under scenarios of climate-change.

1. Introduction

The impact of future climate change on crop production has been widely studied by using crop models and climate change scenarios (Cantelaube and Terres, 2005; Challinor and Wheeler, 2008; Guo et al., 2010; Tao et al., 2008). Future climate scenarios may be beneficial for wheat in some regions, but could reduce productivity in zones where optimal temperatures already exist (Ortiz et al., 2008). The tendency of wheat yield in American Northern Plains will increase 25% in 2030 and 36% in 2095 (Izaurralde et al., 2003). Zhang et al. (2004) indicated that the average wheat production will increase by 9.8% in the North China Plain in the 2090s' B2A scenarios (local sustainability) (Nakicenovic and Swart, 2000). Zhang and Liu (2005) indicated that the future wheat yields will increase 7–58% in the Loess Plateau of China. Winter wheat production in southern Sweden was predicted to increase by 10–20% in 2050 (Eckersten et al., 2001). England wheat production is likely to increase 15–23% in 2050 (Richter and Semenov, 2005). However, wheat yield in southern Australia will decrease about from 13.5% to 32% under most climate change scenarios (Luo et al., 2005).

Evaluation of future climate change research is divided into two groups. The first one is the research for the crop response to the historical climate change (Egli, 2008; Malone et al., 2009; Tao et al., 2006) and the results derived from this group can be used as the basis for making a prediction for crop yields in the future. While the second is, the use of atmospheric circulation model output to drive crop models and can be further subdivided as follows: (1) direct use outputs of GCM or RCM (regional climate model) as the crop model input data (Lin et al., 2005); (2) adjust historical daily meteorological data according to the GCM or RCM outputs results (Daccachea et al., 2011; Liu et al., 2010); (3) adjust the weather generator

* Corresponding author. Tel.: +86 25 84396598; fax: +86 25 84396672.
E-mail addresses: yanzhunjaueducn@163.com, yanzhu@njau.edu.cn (Y. Zhu).

0168-1923/$ – see front matter © 2012 Elsevier B.V. All rights reserved.
http://dx.doi.org/10.1016/j.agrformet.2012.12.008

parameters downscaling of GCM or RCM data to generate daily meteorological data (Semenov and Stratonovitch, 2010; Tao and Zhang, 2011; Trnka et al., 2004; Zhang et al., 2004). 221 papers that used crop simulation models to examine diverse aspects of how climate change might affect agricultural systems were reviewed by White et al. (2011). Only six direct GCM or RCM output was taken as the input of the crop model. 141 papers adjusted historical daily data with outputs of the circulation models. 68 papers adjusted parameters of weather generators such as WGEN or LARS-WG to provide daily weather data which could represent future climates.

The first method has some limitations. Global and regional climate model results cannot directly be used as input for crop models because the output is typically available as monthly means or changes in monthly means of climatic variables (Semenov and Stratonovitch, 2010), but daily time series are needed as input in most crop models. Even if daily output is available, the coarse spatial resolution and large biases, in particular for precipitation is unsuitable for direct use in crop models (Supit et al., 2012). The second method only considers the mean for temperature, rainfall, and radiation, but the standard deviation of these meteorological elements in the future cannot be incorporated. In recent years, the third method has become the most important method for the evaluation of future climate change research. In addition, although GCMs can effectively assess climate change caused by increasing of greenhouse gas emissions, coarse spatial resolution does not reflect reliable regional details. Therefore, downscaled GCMs (Cantelaube and Terres, 2005; Wang et al., 2011) or RCM (Xiong et al., 2007) combined with crop models was used to study the impact of future climate change on crop production in many efforts.

Impact assessment of climate change using crop models can be conducted at either the site or regional scale. At present, evaluation studies at site scale and regional scale are mainly based on the results of several representative agricultural experimental eco-sites (Guo et al., 2010; Zhang et al., 2004). Although it is easy to implement and less time consuming to couple the growing process with environmental variables, the method of using a representative site for a large area or area that has complex spatial heterogeneity can lead to significant simulation errors (Wang et al., 2011). Therefore, the evaluation results with only a few eco-sites cannot represent the characteristics of the region. Comparatively little investigation is based on high-resolution raster data for regional scale evaluation studies (Cantelaube and Terres, 2005; Ramirez-Villegasa et al., 2011; Supit et al., 2012), and mainly for foreign areas.

Many studies have assessed wheat phenology, yield and water use in response to climatic changes in China. Guo et al. (2010) explored the responses of wheat yield and water use efficiency to climate change in the North China Plain, and indicated that wheat yield will increase 9.8% without CO_2 fertilization in 2090s. Liu and Tao (2012) made a probabilistic assessment of changes in wheat yield (based on 5 different climate scenarios) and found that wheat yield would decrease with a probability of more than 69% and 54% under rain-fed and full-irrigation condition with the temperature rising 3°C without CO_2 fertilization. Ju et al. (2005) found that wheat yield would decrease 20% in ten agro-ecological zones of China without CO_2 fertilization in 2070. Tao et al. (2006) explored trends in phenology and yields of wheat in China from 1981 to 2000. Wang et al. (2008) investigated phenological trends in winter wheat in response to climatic changes from 1981 to 2004 in northwest China. Zhang et al. (2011) evaluated changes in evapotranspiration over irrigated winter wheat in North China Plain from 1979 to 2009 and provide references for assessing future ET change. Studies of climate change impacts on wheat in China showed conflicting results and uncertainties primarily relating to differences of sites, crop models, GCM scenarios and managements (Xiong et al., 2009), and above studied mainly explored the responses of wheat yield and water use efficiency to climate change based on site-specific conclusions. A systematic analysis of the relationship between climate change and wheat phenology, yield and water use is essential to assess wheat production risks and water resource allocation at regional scale in the future.

The aim of this paper is to explore the responses of winter wheat phenology, spatial variation of potential and rain-fed production, actual evapotranspiration and IWUE to climate change with the WheatGrow model in China's main wheat production regions and further analyze the reason affecting wheat yield under climate change projections of A2, A1 and B1 in each province, which provides a scientific basis of the future production strategy formulation and the redistribution of agricultural water resources in the wheat producing provinces.

2. Materials and methods

2.1. Study region

Based on the wheat sowing area in 2005 of each county in China obtained from the statistical yearbook, the sowing-area-weighted method (Jagtap and Jones, 2002) was used to aggregate the data of county-level wheat sowing area in 2005 to $0.5^\circ \times 0.5^\circ$ resolution grid-level wheat sowing area, then the ratio of wheat sowing area to total area in each grid was calculated and exhibited in Fig. 1 with ARCGIS 9.2. Ten major production provinces, Jiangsu, Hebei, Henan, Shandong, Shanxi, Shaanxi, Gansu, Hubei, Sichuan and Anhui provinces inside the blue line in Fig. 1A, which have the relatively largest wheat sowing fraction were chosen as study provinces.

The black line in Fig. 1A is the dividing line between winter and spring wheat in Chinese wheat producing regions (Jin, 1996). The regions above the black line are planted to spring wheat, while areas below the black line are planted to winter wheat and were the primary regions for this study. Fig. 1B shows average wheat sowing date (Day of Year, DOY) for the 1998–2003 study regions.

2.2. Data

2.2.1. Generating daily weather

Three GCM models providing the necessary weather variables for WheatGrow model were used in this study. There are the CSIRO-Mk3.5 (Commonwealth Scientific and Industrial Research Organisation Atmospheric Research, Australia, $1.9^\circ \times 1.9^\circ$), ECHam5 (Max Planck Institute for Meteorology, Germany, $1.9^\circ \times 1.9^\circ$) and MIROC3.2 (Center for Climate System Research, National Institute for Environmental Studies, and Frontier Research Center for Global Change, University of Tokyo, Japan, $2.8^\circ \times 2.8^\circ$). GCM generally has a lower spatial resolution. Such a coarse spatial resolution cannot reflect reliable regional detail (Cantelaube and Terres, 2005), therefore it is required to be downscaled in spatial scale for assessing regionally site-specific climatic impacts of climate change on winter wheat. The high-resolution monthly average meteorological data of three GCMs in this study were come from the CIAT database (http://www.ccafs-climate.org/data/) (Ramirez and Jarvis, 2008). The time slices 1990–2010, 2020–2040, 2040–2060 and 2060–2080 were chosen from the GCM data. Three scenarios of A2 (a high-greenhouse-gas-emission scenario), A1 (a low-emissions scenario) and B1 (a medium-emission scenario) are chosen as climate change projections (Nakicenovic and Swart, 2000).

Jones and Thornton (2013) describe a generalized downscaling and data generation method that takes the outputs of a GCM and allows the stochastic generation of daily weather data that are to some extent characteristic of future climatologies. Future

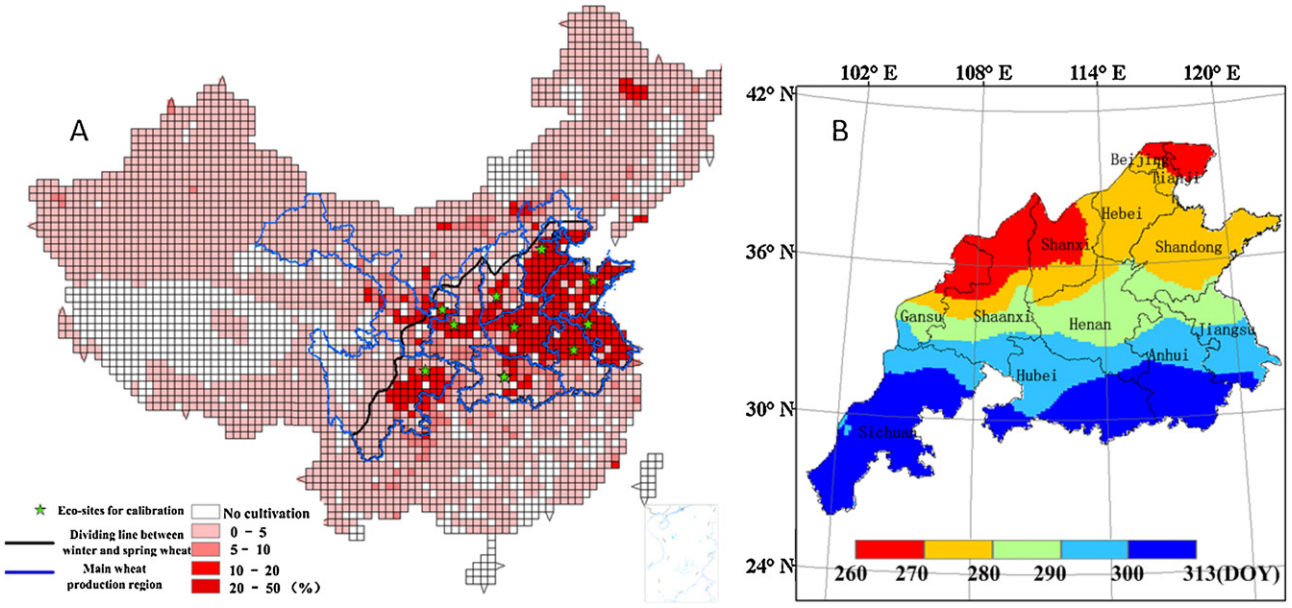

Fig. 1. (A) Distribution map of wheat planting area proportion, main wheat production regions and dividing line between winter and spring wheat. (B) Average sowing date from 1998 to 2003. (For interpretation of references to colour in text, the reader is referred to the web version of this article.)

daily weather data for a total 14,212 grids in our research regions were generated based on Jones's works. The stochastic weather generator MarkSim was used to produce daily weather for each grid cell from the monthly climate data, including maximum and minimum temperature, precipitation, wet days, and solar radiation (Jones and Thornton, 2013). MarkSim is a third-order Markov rainfall generator (Jones and Thornton, 1999, 2000) that has been developed over 20 years. MarkSim divides the world into 720 clusters of climate distinct from one another using 36 values of monthly precipitation and monthly maximum and minimum temperatures, and some of the parameters of the MarkSim model calculated by regression from the cluster most representative of the climate point to be simulated. Jones et al. (2009) generated global regression coefficients of three scenarios for CSIRO-Mk3.5, ECHam5 and MIROC3.2, which can be used to determine to which cluster it belongs and generate daily meteorological data for each grid. The standalone version called MarkSim_alone constructed by Jones is designed for computer users that need to process large amount of data (Jones et al., 2009). The detail for generating daily meteorological data for each grid can be found at (http://www.ccafs-climate.org/media/ccafs_climate/docs/MarkSim_Standalone_Documentation.pdf). 20 set of daily meteorological data, including daily maximum temperature, minimum temperature, solar radiation, rainfall in each gird for the time slices 2000s, 2030s, 2050s, 2070s of GCMs were generated using 20 random seeds.

Due to the regional high-resolution raster data in this study, inconsistency of the meteorological data between adjacent grids may cause a larger spatial variability. However, the current method to generate a downscaling daily meteorological data did not take the spatial correlation between two adjacent grid cells into account (Semenov and Brooks, 1999). In order to ensure the consistency of spatial grid cells on the monthly scale, a bias correction method was used to correct the generated daily meteorological data by calculating the difference between the average of the generated daily meteorological data and raw monthly averages of the climate model.

Corrected daily maximum temperature = daily maximum temperature – (monthly average of generated daily maximum temperature – GCM monthly average maximum temperature)

Corrected daily minimum temperature = daily minimum temperature – (monthly average of generated daily minimum temperature – GCM monthly average minimum temperature)

Corrected daily solar radiation = daily solar radiation – (monthly average of generated daily solar radiation – GCM monthly average solar radiation)

Corrected daily rainfall = daily rainfall/monthly total rainfall (monthly sum of generated daily rainfall/GCM raw monthly total rainfall)

After correction, variation of the generated daily meteorological data by MarkSim does not change, while minimizes the difference between the monthly average of the generated daily meteorological data and the raw GCM monthly meteorological elements. Corrected daily meteorological data in two adjacent grid cells are consistent on monthly scale, which ensure the simulated growth period yield are consistent in two adjacent grid cells as much as possible.

2.2.2. Soil data

The soil data was mainly derived from the Harmonized World Soil Database (HWSD), which was developed and maintained by the International Institute for Applied Systems Analysis (IIASA). Soil textural data of two layers, for 0–30 cm and 30–100 cm, was included in HWSD. The spatial soil information was derived from the ISRIC-WISE (Batjes, 2006) database ($5' \times 5'$), which provided most of the soil parameters (organic Carbon, pH, water storage capacity, soil depth, cation exchange capacity of the soil and the clay fraction, total exchangeable nutrients, lime and gypsum contents, sodium exchange percentage, salinity, textural class and granulometry) required by WheatGrow model within a 100 cm deep soil profile. Wilting point (WP), field capacity (FC) and saturated moisture content (SAT) were estimated by texture and organic matter (Saxton and Rawls, 2006).

2.2.3. Cropping management

WheatGrow model assumes that weeds, diseases, and pests are controlled. The basic carbon dioxide concentrations were 334 ppm when model was constructed. In this research, carbon dioxide concentrations were held constant at 370 ppm which represented the current CO_2 levels for all simulations. Fertilizer was optimally

available in this research. No information about future wheat varieties is available and therefore we assume that wheat types do not change over time. This will show the effects of the changing weather patterns on wheat growth and production.

Irrigation in WheatGrow is applied in 2 ways: (1) automatic irrigation that provides the optimal amount of water to cover the estimated soil water deficiency. During the simulation, irrigation was applied when soil moisture was lower than 65% of field capacity. This implies that water is always available when needed. (2) Rain-fed conditions that no irrigation to supply. For the rain-fed conditions, crops may incur water-stress during long droughts. In this paper we compare rain-fed and irrigated conditions separately. However it can at least direct us to know if the water requirement of crops is fully satisfied and how crops will be affected by climate change. Irrigated and rain-fed conditions are known to influence crop yield differently (Liu et al., 2010), and both are considered in the present study.

Irrigation water use efficiency can be expressed by IWUE (Sun et al., 2010), which can be defined as follows:

$$\mathrm{IWUE} = \frac{(\mathrm{GYi} - \mathrm{GYd})}{I} \quad (1)$$

where GYi is the potential production (kg ha^{-1}), GYd is the rain-fed production (kg ha^{-1}), I is the irrigation amount (mm) in automatic irrigation scenario.

2.2.4. Sowing date

A recent comparison of the thin plate smoothing spline with the geostatistical method (Kriging) showed the close formal connection of both methods (Hutchinson and Gessler, 1994). The main advantage of the splines over geostatistical methods is that the splines do not require prior estimation of the spatial auto-covariance structure, which can be difficult to obtain. In addition, Kriging method requires the data to fit the normal distribution, the sowing date data in this study is not completely accord with the normal distribution. The spline method does not require a regular distribution of data points. A second-order spline using latitude and longitude as independent variables was fitted to interpolate the surfaces of sowing date with the resolution of $0.1^\circ \times 0.1^\circ$. The regional average wheat sowing date of 1998–2003 is shown in Fig. 1B, and the value of each grid is considered as the day of the year (DOY) of wheat sowing. Wheat sowing dates at 148 eco-sites from 2003 to 2005 are use to validate the regional average wheat sowing date of 1998–2003, and the coefficient of determination (R^2) and root mean square error (RMSE) are 0.90 and 4.97 days, respectively (Fig. 2).

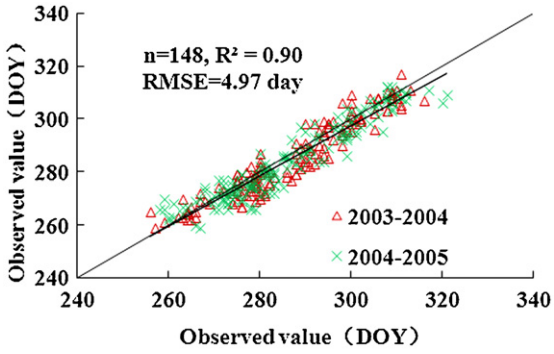

Fig. 2. Validation of the sowing date.

2.3. WheatGrow model description

WheatGrow is mainly composed of five submodels: apical development and phenological development (Yan et al., 2000, 2001); photosynthesis and dry matter production (Liu et al., 2001b); dynamic partitioning (Liu et al., 2001a); organ growth and yield formation (Pan et al., 2007, 2006); soil water balance (Hu et al., 2004a,b, 2005) and N, P, K dynamics (Zhuang et al., 2004). Actual evapotranspiration of winter wheat field was computed by means of the Priestley–Taylor formula. Many studies have made some predictions and evaluations using WheatGrow model at site or regional scale (Huang et al., 2011; Shi et al., 2009; Zhao et al., 2010), and the results showed that the model was able to simulate response of wheat growth and yield to climate and irrigation in China.

2.4. Calibration and validation of the WheatGrow model

When the crop growth model is extended from site to regional scale, the performance of a specific cultivar is of less concerned. Instead, the characteristics of all the cultivars under certain scenarios in the entire region are comprehensively considered as a representative ecotype cultivar for predicting the regional productivity (Iizumi et al., 2009; Shi et al., 2009; Tao et al., 2009). Since the model parameters of the ecotype cultivar are not cultivar-specific but region-specific, the differences between the cultivars within a region could be ignored, and a set of region-specific parameters should be optimized.

In the study region, ten representative eco-sites (Green stars in Fig. 1A), Weifang, Shijiazhuang, Zhengzhou, Huai'an, Hefei, Linfen, Wugong, Xifeng, Bazhong and Zhongxiang, were selected in the province of Shandong, Hebei, Henan, Jiangsu, Anhui, Shanxi, Shaanxi, Gansu, Sichuan, Hubei, to estimate the region-specific

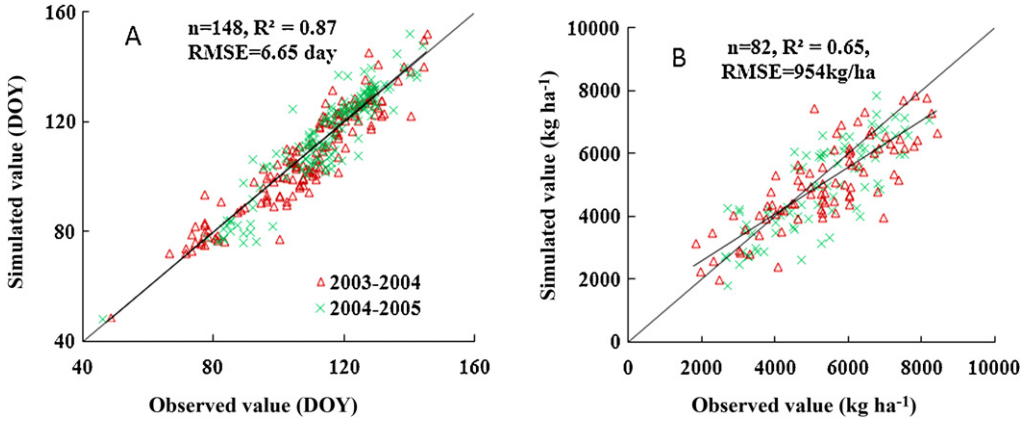

Fig. 3. Validation of the flowering date (A) and yield (B) in regional scale.

Table 1
Cultivar parameters in WheatGrow model.

Provinces	PVT	IE	PS	TS	FDF	SLA	LT	GW	HI	TA
Anhui	30	1.33	0.0060	0.69	0.79	0.0028	46.3	37.02	0.4	0.52
Hebei	37	1.61	0.0068	0.84	0.69	0.0027	63.31	40.5	0.38	0.61
Jiangsu	25	1.68	0.0062	0.67	0.57	0.0026	48.32	44.01	0.38	0.65
Henan	33	1.46	0.0055	1.01	0.82	0.0031	52.27	39.69	0.37	0.46
Gansu	39	1.41	0.0054	0.81	0.69	0.0026	71.94	39.76	0.44	0.47
Shandong	40	1.50	0.0066	0.86	0.74	0.0031	63.69	42.97	0.41	0.54
Hubei	24	1.46	0.0053	1.05	0.70	0.0027	41.42	42.66	0.37	0.63
Sichuan	16	1.03	0.0036	0.40	0.54	0.0024	46.6	37.3	0.39	0.55
Shanxi	37	1.65	0.0072	1.24	0.68	0.0026	82.43	47.06	0.38	0.54
Shaanxi	38	1.64	0.0069	0.96	0.66	0.0032	47.64	31.52	0.36	0.45

PVT: physiological vernalization time/d.
IE: intrinsic earliness.
TS: temperature sensitivity.
PS: photoperiod sensitivity.
FDF: filling duration factor.
SLA: specific leaf area under optimum conditions/ha kg^{-1}.
LT: the max thermal time between two leaves/°C d.
HI: harvest index.
GW: 1000-grain weight/g.
TA: tilling ability.

cultivar parameters (Table 1) with the MCMC-based method (Iizumi et al., 2009) from 1998 to 2003, and 148 other eco-sites were used for validation of the MCMC-based method for estimating region-specific cultivar parameters from 2003 to 2005.

Daily meteorological data was selected for each eco-sites. The soil data including soil physical and chemical properties was selected according to latitude and longitude of eco-sites using GIS. The calibrated regional cultivar parameters at 10 eco-sites above represent the ecotype cultivar of ten provinces respectively. Cropping management was consistent with the actual situation in the field. The R^2 and RMSE between observed and estimated flowering date were 0.87 and 6.65 days, and R^2 and RMSE between observed and estimated yield were 0.65 and 954 kg ha^{-1} (Fig. 3). The estimated values agreed well with the observed values. Therefore, WheatGrow model can be extended to regional scale for accurately predicting the regional wheat production.

2.5. Regional wheat model

This study developed a regional wheat model and decision support system by combining the WheatGrow model with Geographic Information System (GIS) to scale up crop model from site to regional levels. The spatial data in study area is divided into homogeneous grids. The grid is taken as the basic simulation unit, and each grid has a complete set of input data (meteorological, soil, cultivar and management). A total of 14,212 grid cells in main wheat producing regions are simulated under four time slices in 2000s, 2030s, 2050s and 2070s, and then all grid results in one province are aggregated to a regional value. The spatial distribution of flowering date, wheat yield, ET and IWUE are the average of three climate change projections of A2, A1 and B1 of three GCMs.

3. Results

3.1. Projected regional climate changes

Daily average solar radiation, temperature and rainfall were calculated in each grid cell using three GCM models under three different emission scenarios for four time slices. Probability distributions of daily average solar radiation, temperature and rainfall with a total of 14,212 grid cells during the wheat growing season (November to next may) are shown in Fig. 4A–C respectively. Daily average solar radiation in main wheat producing region during the wheat growing season was 9.26 MJ m^{-2} d^{-1}. The probability distributions of accumulated solar radiation during the wheat growing season showed a consistent increased solar radiation from 2000s to 2070s. Daily average temperature in main wheat producing region during the wheat growing season was 7.14 °C. The probability distributions of daily average temperature during the wheat growing season showed a consistent warming trend from 2000s to 2070s. Daily average precipitation in main wheat producing region during the wheat growing season was 1.13 mm. The probability distributions of daily average precipitation during the wheat growing season showed a decreased precipitation from 2000s to 2030s and a consistent increased precipitation from 2030s to 2070s. The probability distributions of daily average solar radiation, temperature and precipitation are highest in A2 scenario, followed by A1 scenario, then B1 scenario.

3.2. Effects on phenology

3.2.1. Flowering date

Wheat flowering date shows an advance trend from north to south and from east to west in main production regions in 2000s. The earliest flowering date was found in Sichuan, followed by Hubei, whereas the latest flowering date was found in the northern part of Gansu, Shanxi, Shaanxi, Hebei (Fig. 5). There was an advance in flowering date in future climate compare to 2000s due to gradually increasing temperature in the future, but with a more homogeneous pattern for the whole producing region. The flowering dates were 3–6, 6–9, and >9 earlier for 2030s, 2050s and 2070s. Wheat flowering date was compared among three different emission scenarios. The earliest flowering date was found from the A2 scenario, followed by A1 scenario, then B1 scenario (Fig. 6). Because the highest rising temperature was found from the A2 scenario, followed by A1 scenario, then B1 scenario.

3.2.2. Grain-filling period

Despite the advance in flowering date, the changes in the reproduction phase (periods after flowering) are relatively stable (Fig. 7). The grain filling period gets slightly shorten in each province. Due to direct correlation between the grain filling stage and wheat production, the shortened grain-filling period may cause the reduction in yield. Yield in the province of Anhui, Jiangsu, Hubei and Sichuan get increased in the future under rain-fed or automatic irrigating conditions, while grain filling period in these provinces did not shorten significantly in the three time slices. Therefore, the slight change of

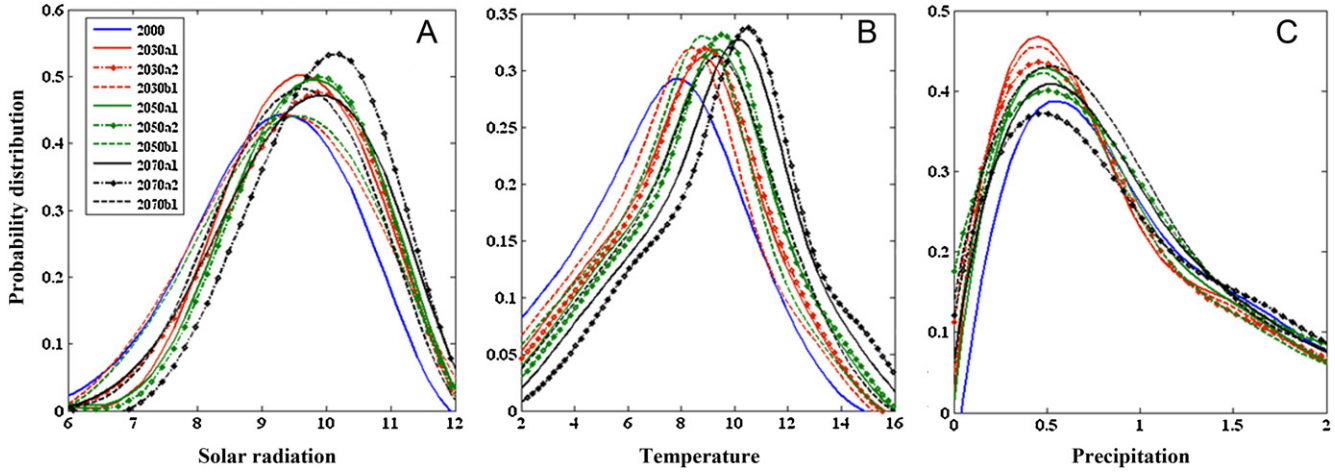

Fig. 4. Probability distributions of daily average meteorological elements during the wheat growing season in main production regions: (A) solar radiation; (B) temperature and (C) precipitation.

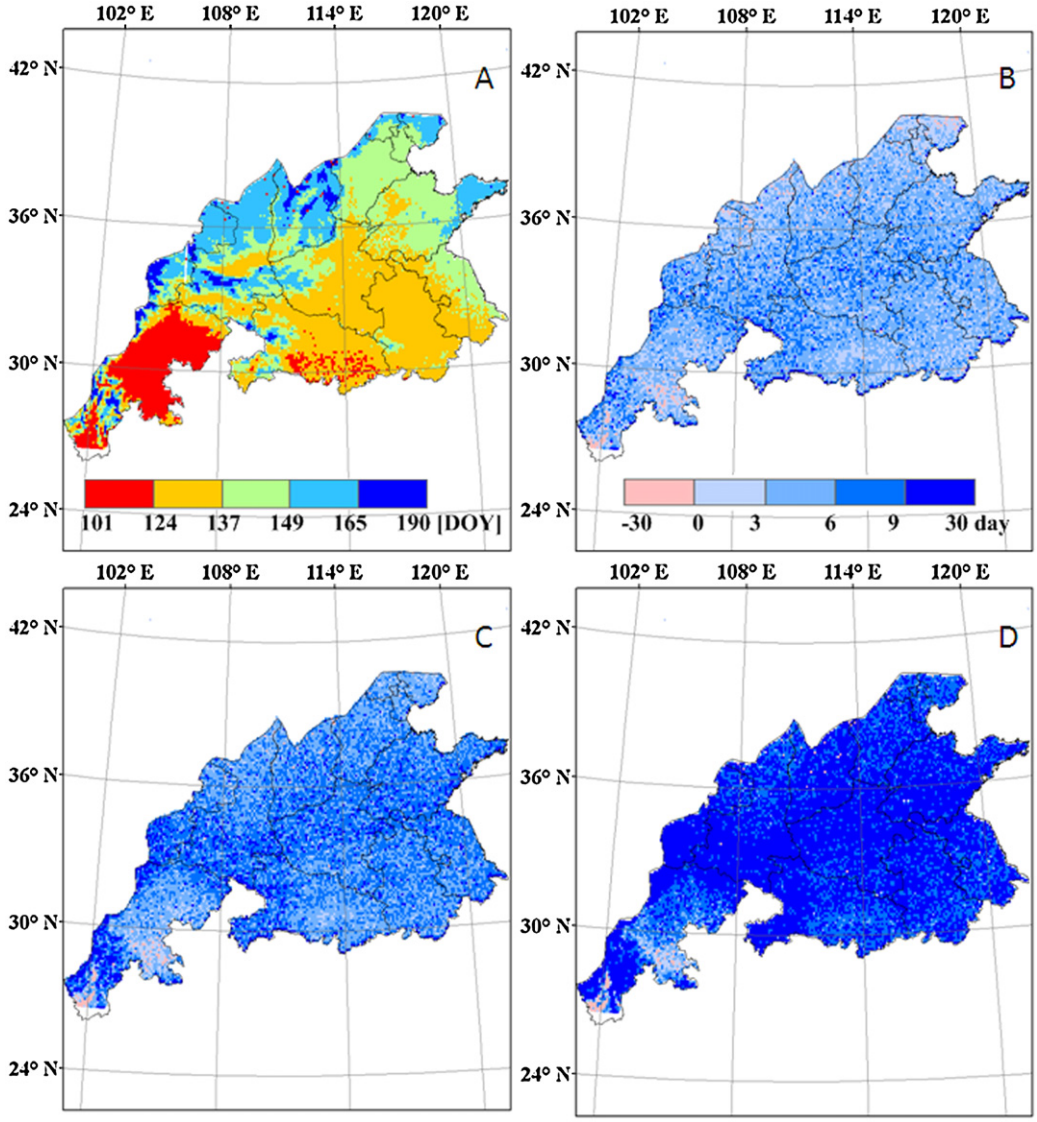

Fig. 5. Simulated wheat flowering date in 2000s (A) and their probable advances in 2030s (B), 2050s (C) and 2070s (D) compare to 2000s. DOY: day of year; (positive values in B–D means the earlier days compare to 2000s).

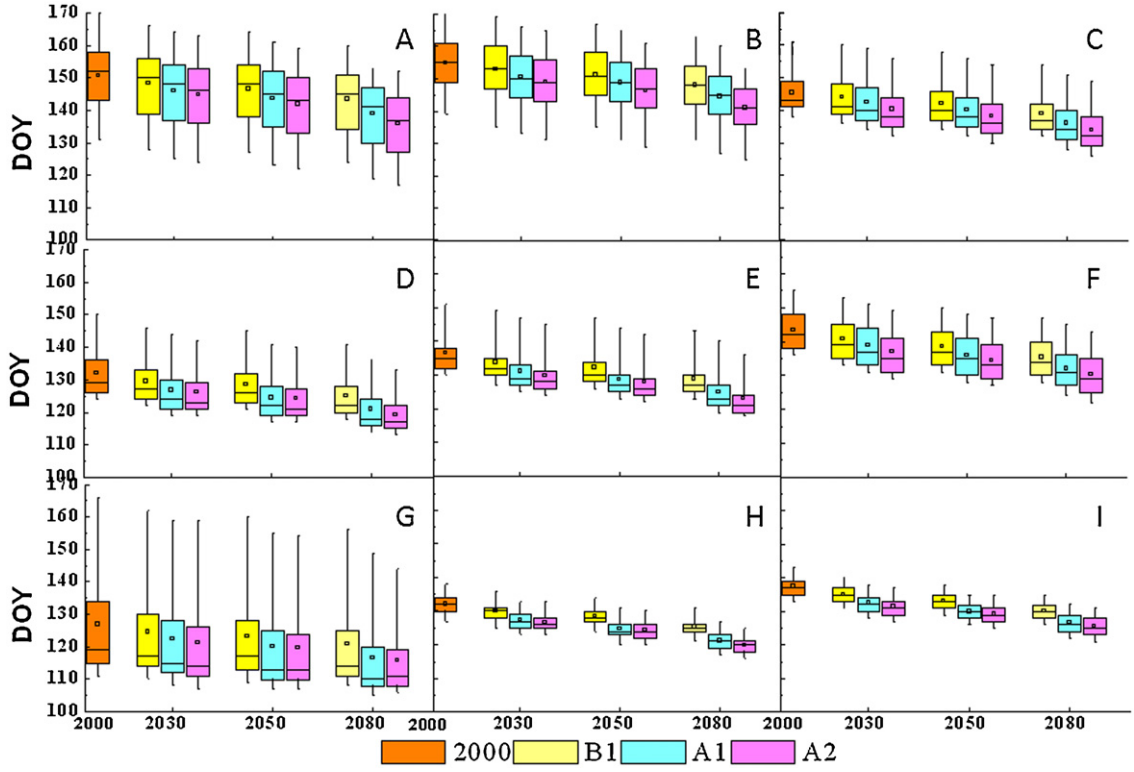

Fig. 6. Simulated wheat flowering dates (DOY) in 2000s, 2030s, 2050s and 2070s in each province under three scenarios of climate-change. (A) Shaanxi and Gansu; (B) Shanxi; (C) Hebei; (D) Hubei; (E) Henan; (F) Shandong; (G) Sichuan; (H) Anhui and (I): Jiangsu. Box boundaries indicate the 25th and 75th percentiles, whiskers below and above the box indicate the 10th and 90th percentiles, the line within the box marks the median, pane in box indicate the mean.

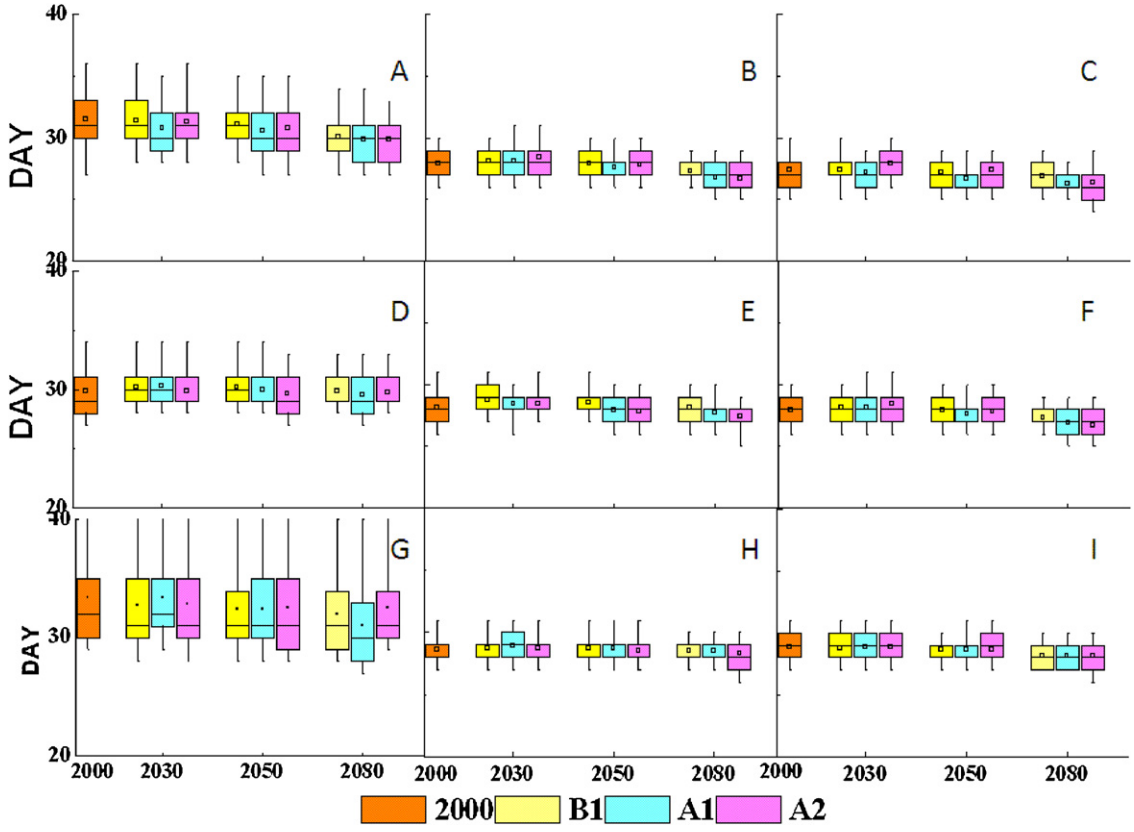

Fig. 7. Simulated wheat grain-filling periods (day) in 2000s, 2030s, 2050s and 2070s in each province under three scenarios of climate-change. (A) Shaanxi and Gansu; (B) Shanxi; (C) Hebei; (D) Hubei; (E) Henan; (F) Shandong; (G) Sichuan; (H) Anhui and (I) Jiangsu. Box boundaries indicate the 25th and 75th percentiles, whiskers below and above the box indicate the 10th and 90th percentiles, the line within the box marks the median, pane in box indicate the mean.

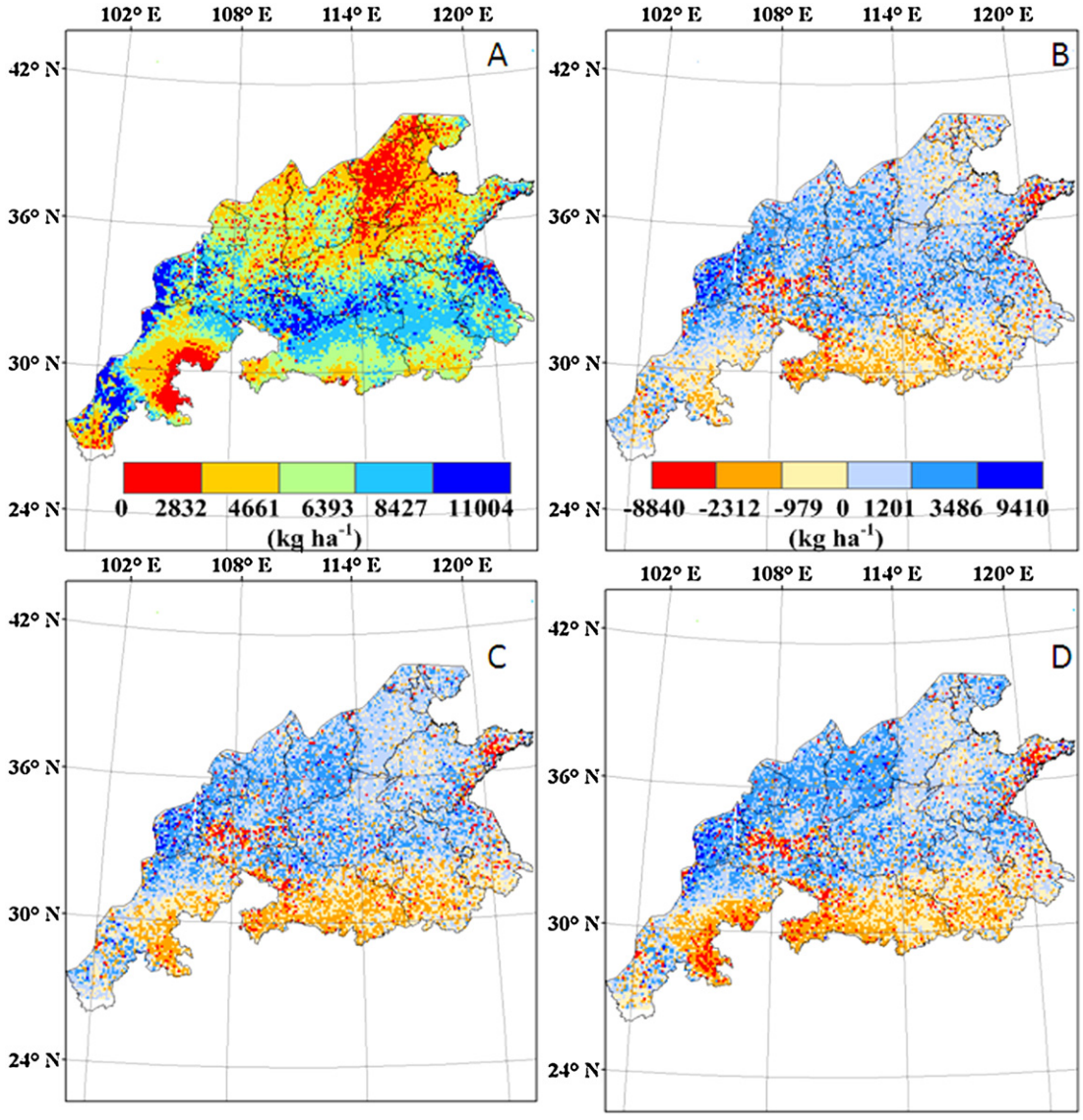

Fig. 8. Simulated wheat yields (kg ha^{-1}) in 2000s (A) and yield changes in 2030s (B), 2050s (C) and 2070s (D) compare to 2000s under three scenarios of climate-change and rain-fed condition (positive values in B–D means the reduced yield compare to 2000s).

grain-filling period will not result in lowering amounts of radiation being intercepted, and lowering biomass production.

3.3. Impacts on yield

3.3.1. Impacts on rain-fed yield

Rain-fed yield first increase and then decrease from north to south in 2000s (Fig. 8), due to rainfall and the shorter growing season caused by higher temperatures in the south. Compared with the 2000s, Rain-fed yield of winter wheat get reduced in 2030s, 2050s and 2070s in the north regions of China (in the north of Qinling Mountains and the Huaihe River), while yield increases of winter wheat are predicted in three future periods in the south region of China. Rain-fed yields showed a constantly increased trend in the province of Sichuan, Hubei, Anhui and Jiangsu, while they will continuously decrease in the province of Shaanxi, Gansu, Shanxi and Hebei (Fig. 9). The simulated yield trends in the province of Shandong and Henan decreased slightly. The simulated yields under three scenarios of climate-change were found to be different. The highest projected yields were found from the A2 scenario in the northern provinces of China, such as Shaanxi, Gansu, Shandong, Hebei, Shanxi and Henan provinces, while the highest projected yield were found from the A1 scenario in the northern provinces of China, such as Jiangsu, Anhui and Sichuan provinces (Fig. 9).

3.3.2. Impacts on full-irrigation yield

Generally, potential yields decrease from north to south, due to lower radiation and the shorter growing season caused by higher temperatures in the south. Assuming enough water is available for irrigation, our results suggest that yields of irrigated winter wheat will increase in almost all regions of the country including those where losses have been predicted under rain-fed conditions (Fig. 10). Due to gradually increasing solar radiation in the future, the higher amounts of solar radiation are intercepted, then the higher amounts of dry matter biomass are produced. The increased winter wheat yields are more obvious in the provinces of Shaanxi, Hebei, Shanxi and Shandong (Fig. 11). The simulated yield trends among three slice times of 2030s, 2050s and 2070s are either not significant or unclear. The simulated yields under three scenarios of climate-change are found to be different. The highest projected yields were found from the A2 scenario, followed by A1 scenario, then B1 scenario.

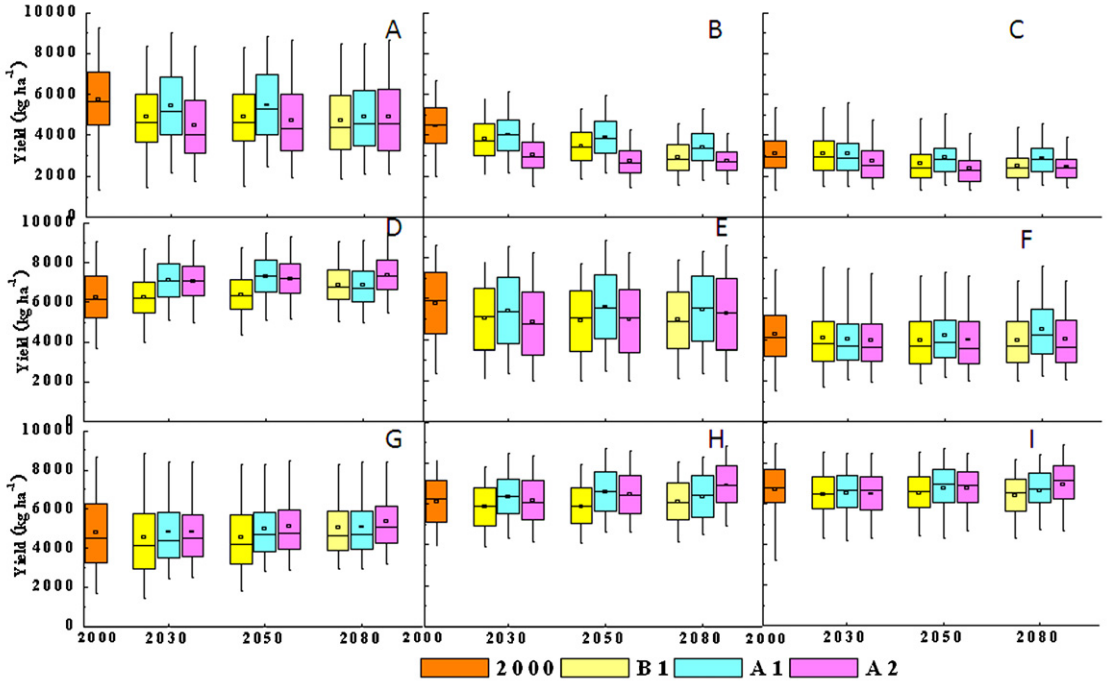

Fig. 9. Simulated wheat yields (kg ha^{-1}) in 2000s, 2030s, 2050s and 2070s in each province under three scenarios of climate-change and rain-fed condition. (A) Shaanxi and Gansu; (B) Shanxi; (C) Hebei; (D) Hubei; (E) Henan; (F) Shandong; (G) Sichuan; (H) Anhui and (I) Jiangsu. Box boundaries indicate the 25th and 75th percentiles, whiskers below and above the box indicate the 10th and 90th percentiles, the line within the box marks the median, pane in box indicate the mean.

3.4. Impacts on cumulative ET

3.4.1. Impacts on cumulative ET in rain-fed conditions

Cumulative ET in winter wheat decreases from south to north in 2000s under rain-fed condition. The cumulative ET during the growing period in winter wheat will decrease in three future periods in response to the warming condition in the north region of China, and increase in the southern region of China (Fig. 12). The spatial pattern of cumulative ET changes is quite similar to that of yield changes (Fig. 12) under rain-fed conditions, suggesting that the factors affecting ET could play a key role in changing wheat yield. The cumulative ET increases with the increasing of temperature and solar radiation, while it decreases due to shorten the phenology of winter wheat and reduced rainfall. The cumulative ET is comprehensively controlled by several climate variables such as temperature, precipitation and solar radiation, which also comprehensively control the wheat yield.

3.4.2. Impacts on cumulative ET in full-irrigation conditions

The cumulative ET in Shandong and Henan province is higher than other provinces under full-irrigation condition in 2000s. The cumulative ET during growing period in winter wheat will increase in three future periods in almost all the provinces. The spatial pattern of cumulative ET changes is also quite similar to that of yield changes (Fig. 13) under full-irrigation condition, suggesting that the factors affecting ET could also play a key role in changing wheat yield. Without considering the effect of water, the cumulative ET increase with the increasing of temperature and solar radiation under full-irrigation conditions.

3.4.3. Relationship between cumulative ET and yield

The largest increases of wheat yield under rain-fed conditions will register in Hubei province. Compared to 2000s, wheat yield will increase by 9.30%, 11.80% and 12.81% in the 2030s, 2050s and 2070s, respectively (Table 2). The corresponding cumulative ET is also the largest, and increases by 1.65%, 3.23% and 5.05% under above three time slices (Table 2). The largest increases of wheat yield under rain-fed conditions will register in Shanxi province. Compared to 2000s, wheat yield will decrease by 18.71%, 24.11% and 31.87% in the 2030s, 2050s and 2070s, respectively. The corresponding cumulative ET is also the largest, and decreases by 9.30%, 11.80% and 12.81% in the 2030s, 2050s and 2070s, respectively. Besides, wheat yield will increase under scenarios of climate-change in all the provinces under full-irrigation condition. The largest increases of wheat yield will register in Hebei province. Compared to 2000s, wheat yield will increase by 17.25%, 21.37% and 26.02% in the 2030s, 2050s and 2070s, respectively. The corresponding cumulative ET is also the largest, and decreases by 3.59%, 5.39% and 8.59% in the 2030s, 2050s and 2070s, respectively.

3.5. Impacts on IWUE

The 2000s' spatial distribution map of wheat irrigation water use efficiency (IWUE) is shown in Fig. 14. Relatively high IWUE is in western Shandong, southern Sichuan, as well as northern Henan, Shanxi and Shaanxi. The IWUE are more than 2.07 kg ha^{-1} mm^{-1} in most parts of those areas. The change of IWUE further decreases under three time slices in 2030s, 2050s and 2070s in western Shandong, southern Sichuan, as well as northern Henan, Shanxi and Shaanxi. IWUE increases under scenarios of climate-change in other areas, especially obvious in central Shaanxi, Gansu and Shandong peninsula. Rainfall haves basically met the water demand for the wheat growth in the most regions of southern China. There are no differences of wheat yield between rain-fed and full-irrigation conditions. Therefore, the IWUE is close to zero. As a result, the limited water should be mad full use of in the regions with relatively high IWUE under scenarios of climate-change.

4. Discussion

The impact of early flowering on potential grain yield is particularly sensitive to changes in temperature (Ludwig and Asseng,

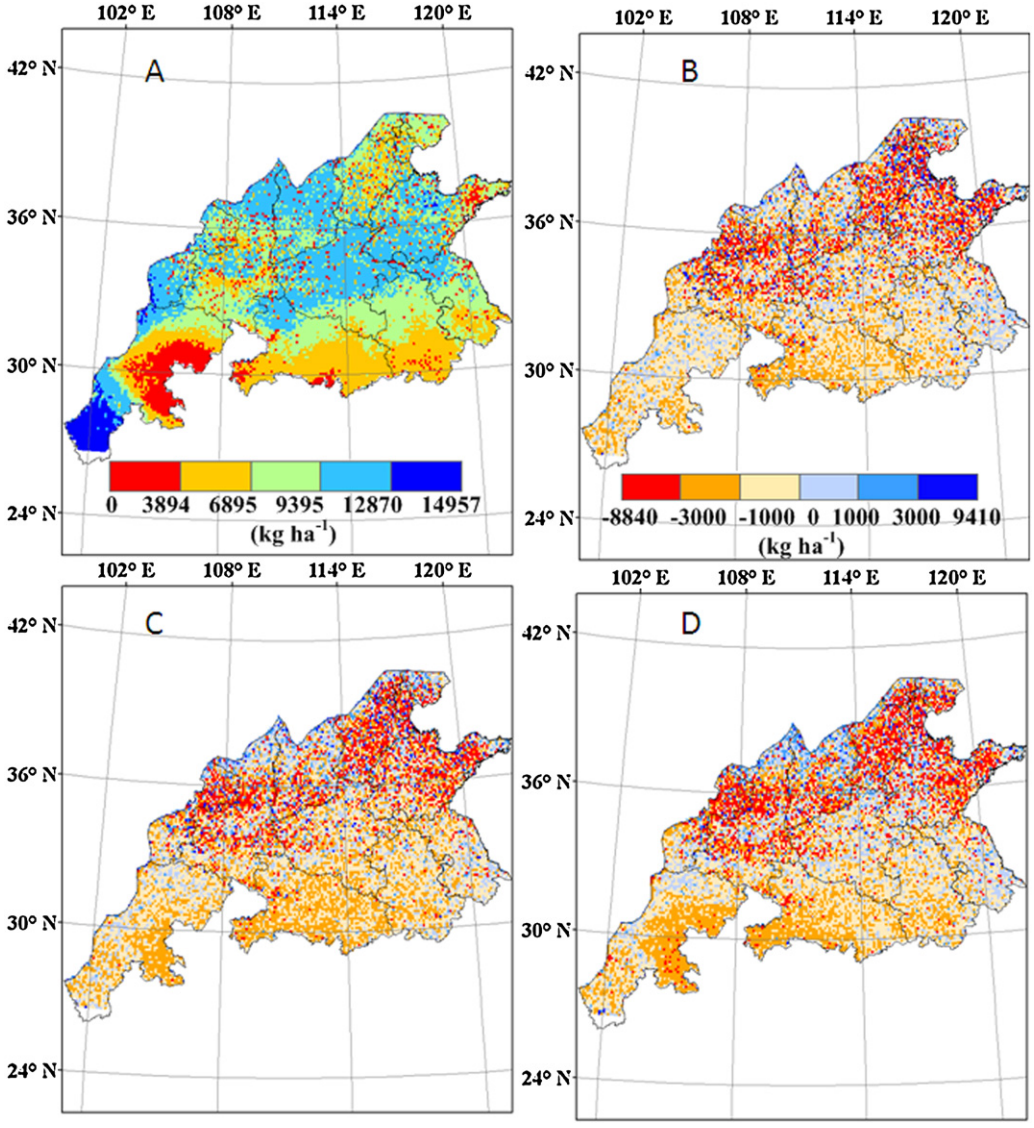

Fig. 10. Simulated wheat yields (kg ha^{-1}) in 2000s (A) and yield changes in 2030s (B), 2050s (C) and 2070s (D) compare to 2000s under three scenarios of climate-change and full-irrigation condition (Positive values in B–D means the reduced yield compare to 2000s).

2010). Because flowering date is governed primarily by temperature, the earlier flowering date indicates warming temperatures in the spring. Further analysis of temperatures by Hu showed that this flowering date shift to earlier time was significantly correlated with the increase in spring season (March–May) daily minimum temperatures (Hu et al., 2005). In addition, an early flowering date results in the advance of the grain filling period, which shifts the grain filling period to a cooler part of the season (Ludwig and Asseng, 2010) and less temperature rise in the entire grain filling period. Therefore, the changes in the grain filling period are

Table 2
Average yield (kg ka^{-1}) and cumulative evapotranspiration (mm) changes in 2030s, 2050s and 2070s compare to 2000s in each province under two irrigation conditions. Negative values in table means the reduced yield or ET compare to 2000s.

Province	2030s				2050s				2070s			
	No irrigation		Irrigation		No irrigation		Irrigation		No irrigation		Irrigation	
	Yield	ET	Yield	ET	Yield	ET	Yield	ET	Yield	ET	Yield	ET
Henan	−11.3	−6.9	8.3	−0.3	−9.8	−5.4	10.0	1.3	−8.9	−3.4	8.6	2.5
Shaanxi-Gansu	−8.1	−7.1	15.3	0.3	−7.6	−6.3	15.8	1.0	−11.2	−5.7	17.0	2.7
Shandong	−5.7	−4.3	16.6	3.0	−5.1	−3.3	20.4	5.0	−2.7	−3.5	20.3	5.1
Shanxi	−18.7	−11.7	8.9	−0.4	−24.1	−12.5	9.2	0.8	−31.9	−13.7	10.6	2.8
Hebei	−5.1	−5.1	17.3	3.6	−15.0	−7.1	21.4	5.4	−16.5	−5.5	26.0	8.6
Jiangsu	−27.7	−15.3	15.2	−1.4	−23.8	−13.0	15.6	−0.6	−26.8	−13.7	19.9	0.9
Sichuan	−2.9	−2.7	6.0	0.2	−0.3	−0.7	9.1	2.4	−0.2	3.4	7.5	6.0
Anhui	−2.1	−2.1	6.8	0.3	0.7	0.0	10.0	2.5	5.1	0.9	13.0	2.8
Hubei	0.3	−0.3	7.5	1.4	3.4	1.5	10.5	3.1	5.7	3.2	10.1	4.0

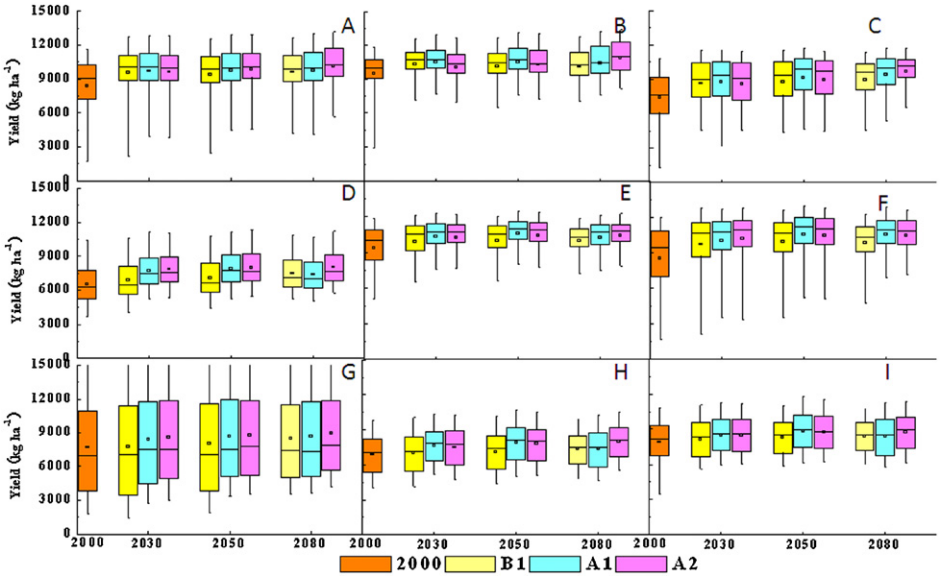

Fig. 11. Simulated wheat yield (kg ha^{-1}) in 2000s, 2030s, 2050s, and 2070s in each province under three scenarios of climate-change and full-irrigation condition. (A) Shaanxi and Gansu; (B) Shanxi; (C) Hebei; (D) Hubei; (E) Henan; (F) Shandong; (G) Sichuan; (H) Anhui and (I) Jiangsu. Box boundaries indicate the 25th and 75th percentiles, whiskers below and above the box indicate the 10th and 90th percentiles, the line within the box marks the median, pane in box indicate the mean.

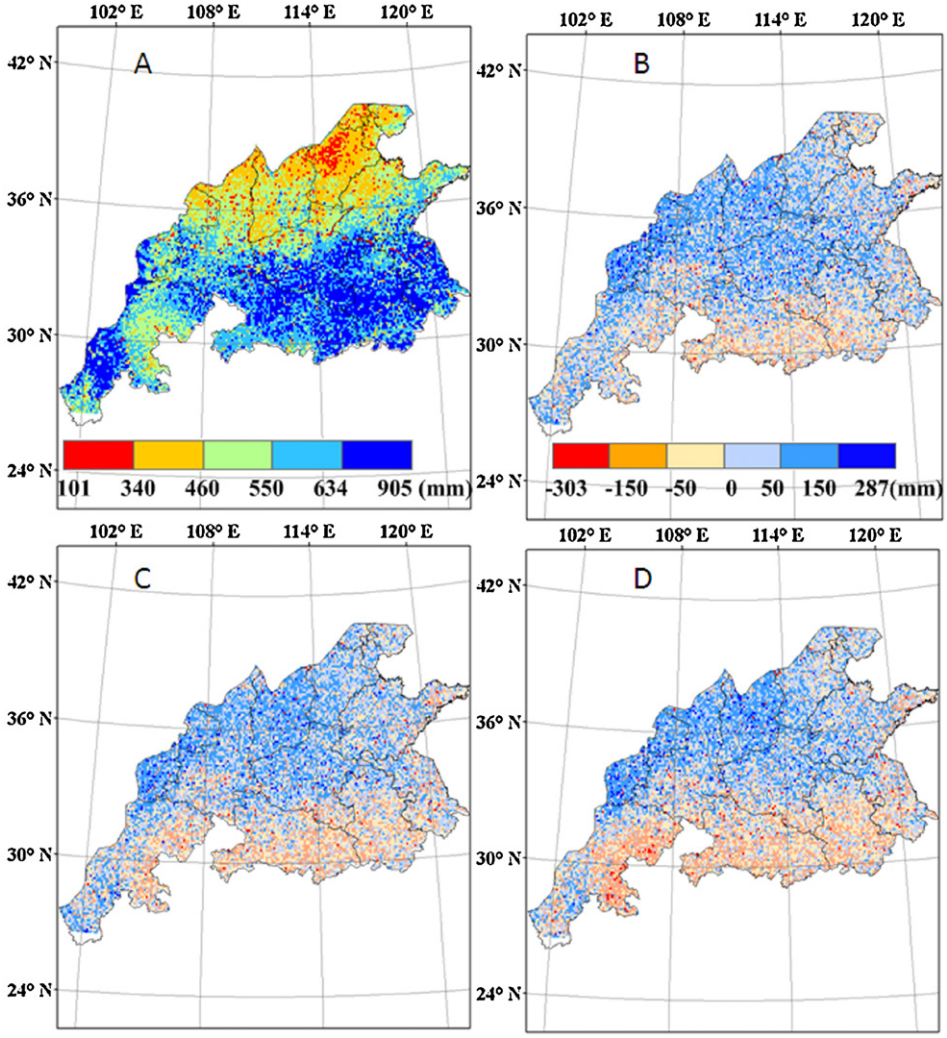

Fig. 12. Simulated wheat cumulative ET (mm) in 2000s (A) and cumulative ET changes in 2030s (B), 2050s (C) and 2070s (D) compare to 2000s under three scenarios of climate-change and rain-fed conditions (positive values in B–D means the reduced ET compare to 2000s).

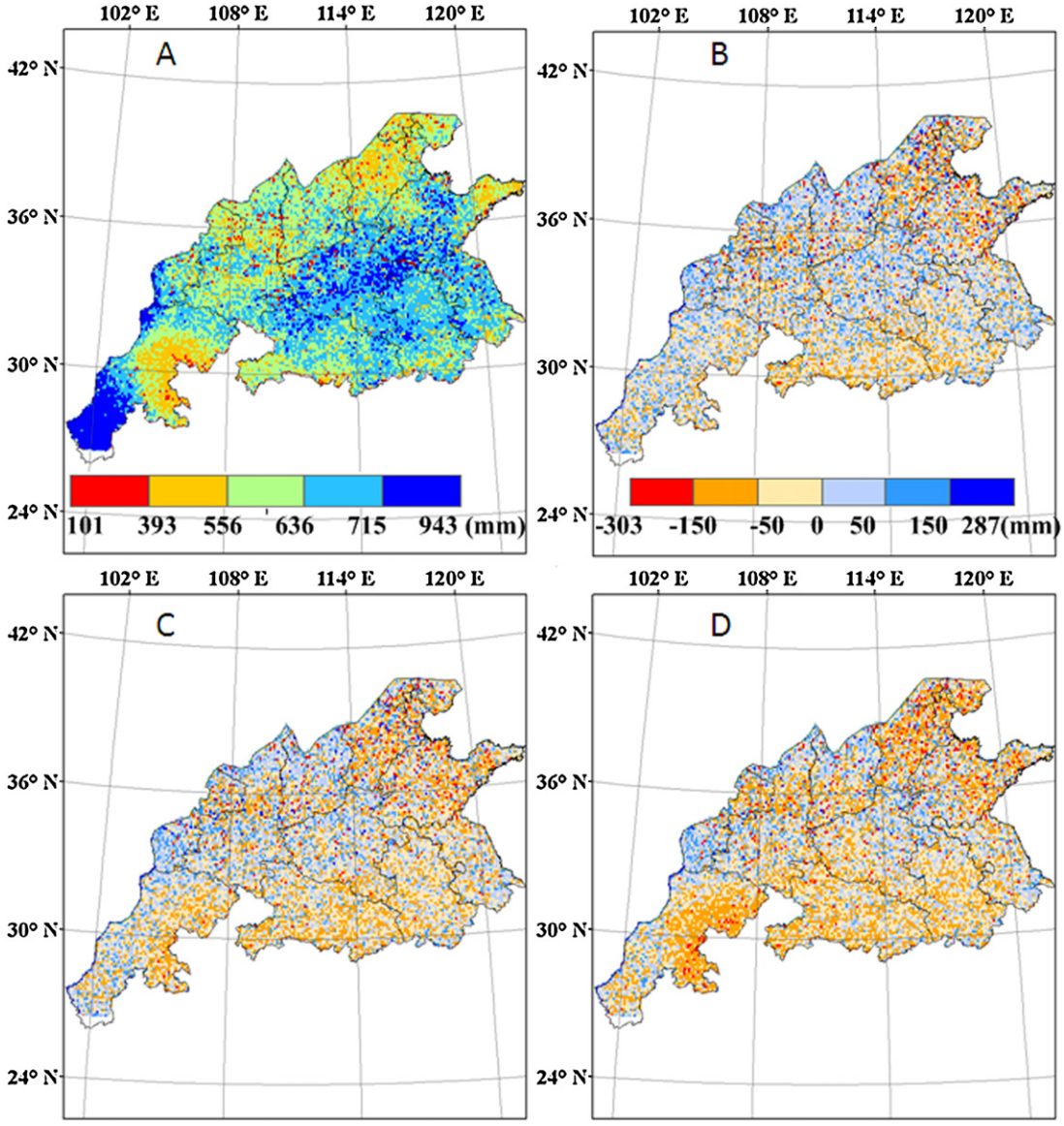

Fig. 13. Simulated wheat cumulative ET (mm) in 2000s (A) and cumulative ET changes in 2030s (B), 2050s (C) and 2070s (D) compare to 2000s under three scenarios of climate-change and full-irrigation conditions (positive values in B–D means the reduced ET compare to 2000s).

relatively stable (Richter and Semenov, 2005) and the negative impact of high temperature on wheat grow in grain filling period have been alleviated to some extent. The advance in flowering dates contributes to most of the changes in wheat phenology. Although an increase in temperature shortens wheat phenology, which will result in lower amounts of radiation being intercepted and lower biomass production, smaller changes in grain filling period may not be the mainly reason for reduction in yield. While some researches (Tao et al., 2009; Wang et al., 2011) were made in other crops show that the great shortened grain-filling period may be the mainly reason for reduction in yield. Besides, full-irrigated winter wheat yields would increase in almost all regions of the country as a result of the increased solar radiation in the future. Rain-fed winter wheat yields showed obvious differences between northern and southern China as a result of the water is the most important limiting factor for wheat production in most parts of northern China but not in the southern China. The decreased precipitation result in the decrease in wheat production in the northern China, while the increased solar radiation during wheat growth periods offsets the decrease in wheat production which is caused by the reason of decreased precipitation in the southern China.

Many studies have reported that the linear relationship exists between wheat yield and cumulative ET (Zhang and Oweis, 1999; Zhang et al., 1999, 2004). The winter wheat yield had a linear relationship with ET, and the correlation coefficient 0.96 and 0.51 ($p < 0.01$) under rain-fed and full-irrigation condition respectively in our research. The results also showed that the change in crop yield was not in proportion to the change in wheat water use. The former was much greater than the latter (Table 2), which means that wheat yield could be significantly improved without much increase in water use (Zhang et al., 2011) and wheat yield could be significantly reduced with less decrease in water use. Therefore, irrigation will improve water use efficiency in the northern areas of China where ET decrease in the future under rain-fall condition. Enough irrigation will make ET keep an increasing tendency, and the wheat yield will be significantly improved in the northern areas of China. If no irrigation or less irrigation, ET may have a decreasing tendency and the wheat yield will be significantly reduced (Chen et al., 2011).

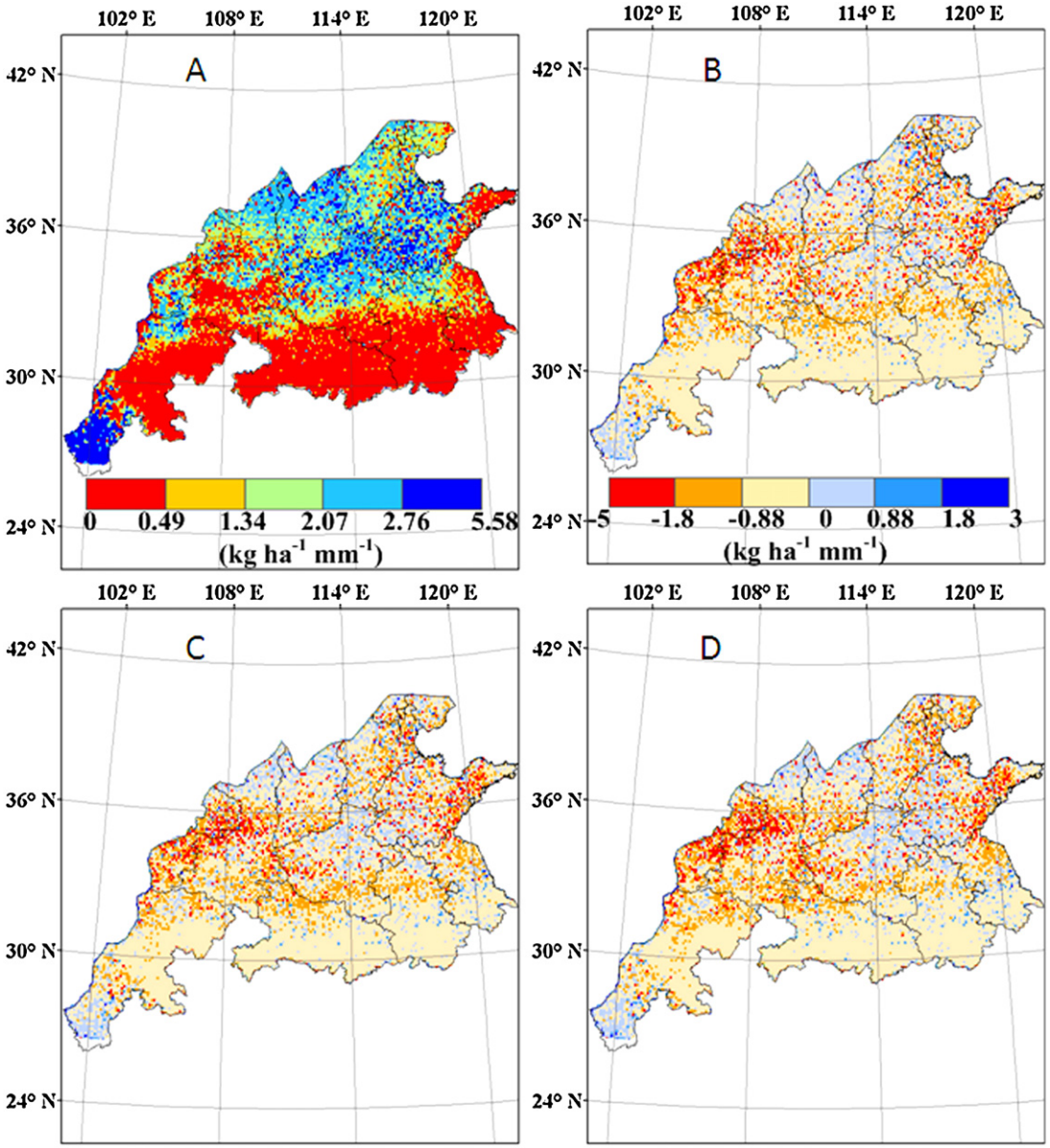

Fig. 14. Simulated wheat irrigation water use efficiency (kg ha^{-1} mm^{-1}) at 2000s (A) and IWUE change in 2030s (B), 2050s (C), and 2070s (D) compare to 2000s under three scenarios of climate-change (positive values in B–D means the reduced IWUE compare to 2000s).

Wheat production was compared among different provinces under full-irrigation conditions. Wheat yield in the northern provinces has increase markedly, which illustrates that wheat production is affected severely by a deficient water supply in the northern China. In addition, IWUE is relatively higher in northern provinces than southern ones. Meanwhile, the changes of IWUE further increase under scenarios of climate-change in most regions of China. Therefore, irrigation water is still the most important factors for China's wheat production. Due to the lack of surface water in northern China, the groundwater has become the main source of irrigation water. To meet the irrigation requirement, groundwater has been over-pumped (Xu et al., 2005). As a consequence, the water table has continuously fallen over the last several decades, creating the so-called "groundwater funnel" in some northern parts which has considerably deteriorated the agricultural sustainability and environmental conditions (Liu et al., 2010). Deficient water supply will reduce the wheat yield significantly. Under future climate conditions, seeking the balance of irrigation water and wheat production requires further study.

5. Conclusions

In this study, the combination of high-resolution GCM models and WheatGrow model were used to assess the effects of climate change on wheat yields in the main wheat production regions of China. Compared with the 2000s, there is an advance in flowering date but with a more homogeneous pattern for the whole producing region. The changes in grain filling period are relatively stable. Under rain-fed conditions, wheat yield gets reduced in the north regions of China in three future periods, while wheat yield will increase in the south regions of China. Under full-irrigation conditions, yields of irrigated winter wheat will increase in almost all areas of whole producing region. The spatial pattern of cumulative ET change is quite similar to that of yield change under rain-fed and full-irrigation conditions. The IWUE decreases under three time slices in 2030s, 2050s and 2070s in western Shandong, southern Sichuan, as well as northern Henan, Shanxi and Shaanxi, while that increases under scenarios of climate-change in most other areas.

Acknowledgements

This research was supported by the National Natural Science Foundation of China (31271616), the National High-Tech Research and Development Plan of China (2013AA100404), the National Science and Technology Support Program of China (2011BAD21B03) and Advantages Discipline Construction Project Funded Projects of Jiangsu Universities (PAPD).

References

Batjes, N.H., 2006. ISRIC-WISE Derived Soil Properties on a 5 by 5 Arc-minutes Global Grid. International Soil Reference and Information Centre (ISRIC), Wageningen, the Netherlands.
Cantelaube, P., Terres, J.M., 2005. Seasonal weather forecasts for crop yield modelling in Europe. Tellus A 57A, 476–487.
Challinor, A.J., Wheeler, T.R., 2008. Crop yield reduction in the tropics under climate change. Processes and uncertainties. Agr. Forest. Meteorol. 148, 343–356.
Chen, C., Baethgen, W., Wang, E., Yu, Q., 2011. Characterizing spatial and temporal variability of crop yield caused by climate and irrigation in the North China Plain. Theor. Appl. Climatol. 106 (3), 365–381.
Daccachea, A., Weatherheada, E.K., Stalhamb, M.A., Knoxa, J.W., 2011. Impacts of climate change on irrigated potato production in a humid climate. Agr. Forest Meteorol. 151, 1641–1653.
Eckersten, H., Blombäck, K., Kätterer, T., Nyman, P., 2001. Modelling C, N, water and heat dynamics in winter wheat under climate change in southern Sweden. Agr. Ecosyst. Environ. 86 (3), 221–235.
Egli, D.B., 2008. Soybean yield trends from 1972 to 2003 in mid-western USA. Field Crop Res. 106 (1), 53–59.
Guo, R., Lin, Z., Mo, X., Yang, C., 2010. Responses of crop yield and water use efficiency to climate change in the North China Plain. Agr. Water Manage. 97, 1185–1194.
Hu, J.C., Cao, W.X., Jiang, D., 2004a. Quantification of water stress factor for crop growth simulation effects of drought and waterlogging stress on photosynthesis, transpiration and dry matter partitioning in winter wheat. Acta Agron. Sin. 30 (4), 315–320.
Hu, J., Cao, W., Luo, W., Zhu, Y., 2004b. Quantification of water stress factor for crop growth simulation II. Model establishment and validation. Acta Agron. Sin. 30 (5), 460–464.
Hu, Q., Weiss, A., Feng, S., Baenziger, P.S., 2005. Earlier winter wheat heading dates and warmer spring in the U.S. Great Plains. Agr. Forest Meteorol. 135, 284–290.
Huang, Y., Zhu, Y., Wang, H., Yao, X., Cao, W., Hannaway, D.B., Tian, Y., et al., 2011. Predicting winter wheat growth based on integrating remote sensing and crop growth modeling techniques. Acta Ecol. Sin. 31 (4), 1073–1084.
Hutchinson, M.F., Gessler, P.E., 1994. Splines-more than just a smooth interpolator. Geoderma 45, 45–67.
Iizumi, T., Yokozawa, M., Nishimori, M., 2009. Parameter estimation and uncertainty analysis of a large-scale crop model for paddy rice: application of a Bayesian approach. Agr. Forest Meteorol. 149 (2), 333–348.
Izaurralde, R.C., Rosenberg, N.J., Brown, R.A., Thomson, A.M., 2003. Integrated assessment of Hadley Center (HadCM2) climate-change impacts on agricultural productivity and irrigation water supply in the conterminous United States Part II. Regional agricultural production in 2030 and 2095. Agr. Forest Meteorol. 117, 97–122.
Jagtap, S.S., Jones, J.W., 2002. Adaptation and evaluation of the CROPGRO-soybean model to predict regional yield and production. Agr. Ecosyst. Environ. 93 (1-3), 73–85.
Jin, S., 1996. China Wheat. China Agricultural Press, Beijing.
Jones, P.G., Thornton, P.K., 1999. Fitting a third-order Markov rainfall model to interpolated climate surfaces. Agr. Forest Meteorol. 97, 213–231.
Jones, P.G., Thornton, P.K., 2000. MarkSim: software to generate daily weather data for Latin America and Africa. Agron. J. 92, 445–453.
Jones, P.G., Thornton, P.K., Heinke, J., 2009. Generating characteristic daily weather data using downscaled climate model data from the IPCC's Fourth Assessment Report, CGIAR Research Program on Climate Change, Agriculture and Food Security (CCAFS); Waen Associates; International Livestock Research Institute (ILRI); Potsdam Institute for Climate Impact Research (PIK).
Jones, P.G., Thornton, P.K., 2013. Generating downscaled weather data from a suite of climate models for agricultural modelling applications. Agr. Syst. 114 (1–5), http://dx.doi.org/10.1016/j.agsy.2012.08.002.
Ju, H., Xiong, W., Xu, Y.L., Lin, E.D., 2005. Impacts of climate change on wheat yield in China. Acta Agron. Sin. 31 (10), 1340–1343.
Lin, E., et al., 2005. Climate change impacts on crop yield and quality with CO_2 fertilization in China. Philos. Trans. Roy. Soc. 360, 2149–2154.
Liu, S., et al., 2010. Crop yield responses to climate change in the Huang-Huai-Hai Plain of China. Agr. Water Manage. 97, 1195–1209.
Liu, T., Cao, W., Luo, W., 2001a. Quantitative simulation on dry matter partitioning dynamic in wheat organs. J. Triticeae Crops 21 (1), 25–31.
Liu, T., Cao, W., Luo, W., 2001b. A simulation model of photosynthetic production and dry matter accumulation in wheat. J. Triticeae Crops 21 (3), 26–30.
Liu, Y., Tao, F., 2012. Probabilistic assessment and uncertainties analysis of climate change impacts on wheat biomass. Inst. Geogr. Sci. Nat. Resour. Res. 67 (3), 337–345.
Ludwig, F., Asseng, S., 2010. Potential benefits of early vigor and changes in phenology in wheat to adapt to warmer and drier climates. Agr. Syst. 103, 127–136.
Luo, Q., Bellotti, W., Williams, M., Bryan, B., 2005. Potential impact of climate change on wheat yield in South Australia. Agr. Forest Meteorol. 132, 273–285.
Malone, R.W., et al., 2009. Quasi-biennial corn yield cycles in Iowa. Agr. Forest Meteorol. 149, 1087–1094.
Nakicenovic, N., Swart, R. (Eds.), 2000. Special Report on Emission Scenarios. Cambridge University Press, Cambrige, UK.
Ortiz, R., et al., 2008. Climate change: can wheat beat the heat? Agr. Ecosyst. Environ. 1269, 46–58.
Pan, J., Zhu, Y., Cao, W., 2007. Modeling plant carbon flow and grain starch accumulation in wheat. Field Crop Res. 101, 276–284.
Pan, J., et al., 2006. Modeling plant nitrogen uptake and grain nitrogen accumulation in wheat. Field Crop Res. 97, 322–336.
Ramirez-Villegasa, J., Jarvis, A., Läderachd, P., 2011. Empirical approaches for assessing impacts of climate change on agriculture: the EcoCrop model and a case study with grain sorghum. Agr. Forest. Meteorol., http://dx.doi.org/10.1016/j.agrformet.2011.09.005.
Ramirez, J., Jarvis, A., 2008. High Resolution Statistically Downscaled Future Climate Surfaces. International Center for Tropical Agriculture (CIAT), International Center for Tropical Agriculture (CIAT); CGIAR Research Program on Climate Change, Agriculture and Food Security (CCAFS), Cali, Colombia.
Richter, G.M., Semenov, M.A., 2005. Modelling impacts of climate change on wheat yields in England and Wales: assessing drought risks. Agr. Syst. 84, 77–97.
Saxton, K.E., Rawls, W.J., 2006. Soil water characteristic estimates by texture and organic matter for hydrologic solutions. Soil Sci. Soc. Am. J. 70, 1569–1578.
Semenov, M.A., Brooks, R.J., 1999. Spatial interpolation of the LARS-WG stochastic weather generator in Great Britain. Clim. Res. 11, 137–148.
Semenov, M.A., Stratonovitch, P., 2010. Use of multi-model ensembles from global climate models for assessment of climate change impacts. Clim. Res. 41, 1–14.
Shi, X., Tang, L., Liu, X., Cao, W., Zhu, Y., 2009. Predicting spatial productivity in wheat based on model and GIS. Sci. Agr. Sin. 42, 3828–3835.
Sun, H., et al., 2010. Effect of precipitation change on water balance and WUE of the winter wheat–summer maize rotation in the North China Plain. Agr. Water Manage. 97, 1139–1145.
Supit, I., et al., 2012. Assessing climate change effects on European crop yields using the crop growth monitoring system and a weather generator. Agr. Forest Meteorol. 164, 96–111.
Tao, F., Hayashi, Y., Zhang, Z., Sakamoto, T., Yokozawa, M., 2008. Global warming, rice production, and water use in China: Developing a probabilistic assessment. Agr. Forest Meteorol. 148, 94–110.
Tao, F., Yokozawa, M., Xu, Y., Hayashi, Y., Zhang, Z., 2006. Climate changes and trends in phenology and yields of field crops in China, 1981–2000. Agr. Forest Meteorol. 138, 82–92.
Tao, F., Yokozawa, M., Zhang, Z., 2009. Modelling the impacts of weather and climate variability on crop productivity over a large area: a new process-based model development, optimization, and uncertainties analysis. Agr. Forest Meteorol. 149 (5), 831–850.
Tao, F., Zhang, Z., 2011. Impacts of climate change as a function of global mean temperature: maize productivity and water use in China. Clim. Change 105, 409–432.
Trnka, M., Dubrovsky, M., Semeradova, D., Zalud, Z., 2004. Projections of uncertainties in climate change scenarios into expected winter wheat yields. Theor. Appl. Climatol. 77, 229–249.
Wang, H.L., et al., 2008. Phenological trends in winter wheat and spring cotton in response to climate changes in northwest China. Agr. Forest Meteorol. 148, 1242–1251.
Wang, M., Li, Y., Ye, W., Bornman, J.F., Yan, X., 2011. Effects of climate change on maize production, and potential adaptation measures: a case study in Jilin Province, China. Clim. Res. 46, 223–242.
White, J.W., Hoogenboom, G., Kimballa, B.A., Walla, G.W., 2011. Methodologies for simulating impacts of climate change on crop production. Field Crop Res. 124, 357–368.
Xiong, W., Holman, I., Lin, E., Conway, D., Jiang, J., Xu, Y., Li, Yan, 2009. Future cereal production in China: the interaction of climate change, water availability and socio-economic scenarios. Global Environ. Change 19, 34–44.
Xiong, W., Matthews, R., Holman, I., Lin, E., Xu, Y., 2007. Modelling China's potential maize production at regional scale under climate change. Clim. Change 85, 433–451.
Xu, Y., Mo, X., Cai, Y., Li, X., 2005. Analysis on groundwater table drawdown by land use and the quest for sustainable water use in the Hebei Plain in China. Agr. Water Manage. 75 (1), 38–53.
Yan, M., Cao, W., Luo, W., 2000. A mechanistic model of phasic and phenological development of wheat I. Assumption and description of the model. Chin. J. Appl. Ecol. 11 (3), 355–359.
Yan, M.C., Cao, W.X., Luo, W.H., Li, C.D., 2001. A simulation model of shoot apex primordium development in wheat. Acta Agron. Sin. 27 (3), 356–362.
Zhang, H., Oweis, T., 1999. Water–yield relations and optimal irrigation scheduling of wheat in the Mediterranean region. Agr. Water Manage. 38, 195–211.
Zhang, H., Wang, X., You, M.Z., Liu, C.M., 1999. Water–yield relations and water-use efficiency of winter wheat in the North China Plain. Irrig. Sci. 19, 37–45.
Zhang, X.C., Liu, W.Z., 2005. Simulating potential response of hydrology soil erosion, and crop productivity to climate change in Changwu tableland region on the Loess Plateau of China. Agr. Forest Meteorol. 131, 127–142.

Zhang, X.C., Nearing, M.A., Garbrecht, J.D., Steiner, J.L., 2004. Downscaling monthly forecasts to simulate impacts of climate change on soil erosion and wheat production. Soil Sci. Soc. Am. J. 68, 1376–1385.
Zhang, X., Chen, S., Sun, H., Shao, L., Wang, Y., 2011. Changes in evapotranspiration over irrigated winter wheat and maize in North China Plain over three decades. Agr. Water Manage. 98, 1097–1104.
Zhao, Y., Tang, L., Cao, W., Zhu, Y., 2010. Adaptability evaluation of a wheat growth model (WheatGrow). J. Triticeae Crops 30 (3), 443–448.
Zhuang, H.Y., Cao, W.X., Jiang, S.X., 2004. Simulation on nitrogen uptake and partitioning in crops. Syst. Sci. Compr. Stud. Agric. 20 (1), 5–11.